

Supporting Information

3D Hierarchical Porous Structured Carbon Nanotube Aerogel-Supported Sn Spheroidal Particles: An Efficient and Selective Catalyst for Electrochemical Reduction of CO₂ to Formate

Zhipeng Chen^{a, b}, Shunyu Yao^a, Licheng Liu^{a, *}

^a CAS Key Laboratory of Bio-based Materials, Qingdao Institute of Bioenergy and Bioprocess Technology, Chinese Academy of Sciences, Qingdao 266101, Shandong, China

^b University of Chinese Academy of Sciences, Beijing 100049, China

*Corresponding author: Email: liulc@qibebt.ac.cn; Tel: +86-532-80662780

Table of Contents

Index	Page
Synthesis of Sn/CNT-Agls and Sn/CNT	S2
Electrodes preparation	S3
Electrochemical experiments	S3
Characterization and Analysis.	S3-S4
Figure S1. Typical SEM images of Sn/CNT and Sn/CNT-Agls	S5
Figure S2. The morphology of the Sn particles supported on the CNT-Agls before and after the electrolysis experiment.	S6
Figure S3. Typical TEM images of Sn/CNT-Agls and the plot of Sn particles size distribution	S7
Figure S4. XRD patterns of the Sn/CNT and Sn/CNT-Agls samples	S7
Figure S5. Survey XPS spectrum of Sn/CNT-Agls and Sn/CNT.	S8
Figure S6. High-resolution Sn 3d XPS spectrum of Sn/CNT-Agls sample	S8
Figure S7. CVs of Sn/CNT-Agls/CC electrode at different sweep rate and the variations of peak current densities with the sweep rates.	S9

Figure S8. Comparison catalytic activity on CNTs/CC, CNT-Agls/CC, Sn/CNT/CC and Sn/CNT-Agls/CC electrodes at -0.96 V	S10
Table S1. Comparison of electrocatalytic activity for electrochemical reduction of CO ₂ to formate on Sn-based electrodes	S11
References	S12

Experimental Section

Synthesis of Sn/CNT-Agls and Sn/CNT. The 3D structured Sn/CNT-Agls electrocatalyst was fabricated by a three-step process of chemical crosslinking, freeze drying and roasting reduction. In a typical experiment, 50 mg chitosan (CS) was dissolved in 10 mL of 1% acetic acid solution (V: V ratio = 1: 99) under stirring and heating at 50 °C for 60 min to achieve the 0.5 wt.% CS solution firstly. At the same time, 250 mg multi-wall carbon nanotube (MWCNT) and 3.5 g SnCl₄·5H₂O were dispersed in 50 mL deionized water, strongly sonicated for 10 min to form the 0.2 M stable hybrid dispersion of CNT and Sn(OH)_x. Subsequently, a 10 mL of 0.5 wt.% CS solution was mixed with 50 mL of 0.2 M CNT and Sn(OH)_x hybrid dispersion, sonicated for 5 min to prepare the stable hybrid suspension of CNTs, CS and Sn(OH)_x. Afterwards, the hybrid suspension was dispensed into a 10 mL vials, and subsequently frozen under -25 °C for 12 h. After that, the sample was freeze-dried at -80 °C for 48 h to obtain Sn(OH)_x /CNT-Agls. Finally, the as-prepared SnCl₄/CNT-Agls was converted to Sn/CNT-Agls via a simple roasting reduction process under H₂ atmosphere at 400 °C for 5h. For comparison, the Sn/CNT was synthesized as the following procedures. Firstly, the 0.2 M stable hybrid aqueous dispersion of CNT and Sn(OH)_x was prepared as the same procedure above and then dried at 80 °C for 24 h. Subsequently, the as-prepared Sn(OH)_x/CNT-Agls composite was converted to Sn/CNT through the same process of roasting reduction.

Electrodes preparation. A substrate electrode was fabricated by carbon cloth (abbreviated to CC, 1×1cm, 0.03 cm), which was sonicated by 5 M hydrochloric acid, acetone and deionized water for 15 min, respectively. 2.0 mg Sn/CNT-Agls (the content of Sn is 79.8 wt.%) or Sn/CNT sample was mixed with the 120 μ L of 5 wt.% PVDF binder by full grinding and then was coated on the electrode. Subsequently, the obtained Sn/CNT-Agls/CC and Sn/CNT/CC electrode were vacuum dried at 45 °C for 12 h, removed and set aside.

Electrochemical experiments. A three electrode test was carried out in a sealed H-cell which was separated by Nafion N117 membrane. The Sn/CNT-Agls/CC electrode or Sn/CNT/CC was used as the working electrode. The reference and counter electrodes are Ag/AgCl and Pt plate (1×1cm), respectively. A CHI630C electrochemical analyzer (Shanghai Chenhua instrument co. LTD, China) was used in all the electrochemical experiments. Cyclic voltammetry (CV) and Constant potential electrolysis (i-t) experiments were performed in 0.5 M KHCO₃. Before the experiments, constant bubbling N₂ (99.99%) and CO₂ (99.99%) for 30 min to remove O₂ from the H-cell and electrolyte solution. The flow rate of CO₂ was 40 mL min⁻¹ in the process of CO₂ reduction. Current density (*j*) was determined on the geometrical area of the working electrode (1 cm²). All the experiments were studied at atmospheric pressure and room temperature (25 ± 3 °C) and all potentials reported in this paper are with respect to reversible hydrogen electrode (RHE).

Characterization and Analysis. Scanning electron microscope (SEM) pictures were obtained through the Hitachi S-4800 high-resolution electron microscope without any conductive coating.

X-ray diffraction (XRD) patterns were obtained on the D8 advance X-ray Diffractometer from Bruker with Cu K α radiation ($\lambda = 1.541 \text{ \AA}$). The XRD was recorded in the range of 10 to 80 degrees, with degree steps of 0.02 and acquisition times of 0.1 s step⁻¹.

X-ray photoelectron spectroscopy (XPS) was carried out on a PHI Quantera SXM spectrometer with a monochromator and Al anode target at 40 kV. All the binding

energy corresponds to the standard C1s peak at 284.8 eV in this experiment.

N₂ adsorption-desorption isotherms measurements were performed on a Micromeritics ASAP 2020M. The multiple-point BET method was used to calculate the specific surface areas of the catalysts and the pore size distribution was obtained by Barrett Joyner Halenda (BJH) method.

Liquid phase products were quantified by a high performance liquid chromatography (HPLC, Agilent 1200) with the Aminex HPX-87H Ion Exclusion columns. The mobile phase was 5 mM H₂SO₄ and injection rate was 0.5 mL min⁻¹. The amount of measurement was 10 μL every time.

Faradaic efficiency (η) of formate production was achieved by the formula:

$$\eta = 2nF / Q$$

where η is Faradaic efficiency of formate; 2 represents the number of electrons required to form formate from CO₂; n represents the total number of moles of formate production, which was measured by HPLC; F represents Faraday constant (96485); and the Q corresponds to the amount of cumulative charge in the process of CO₂ reduction, which was provided by the electrochemical workstation.

Supplementary Figures

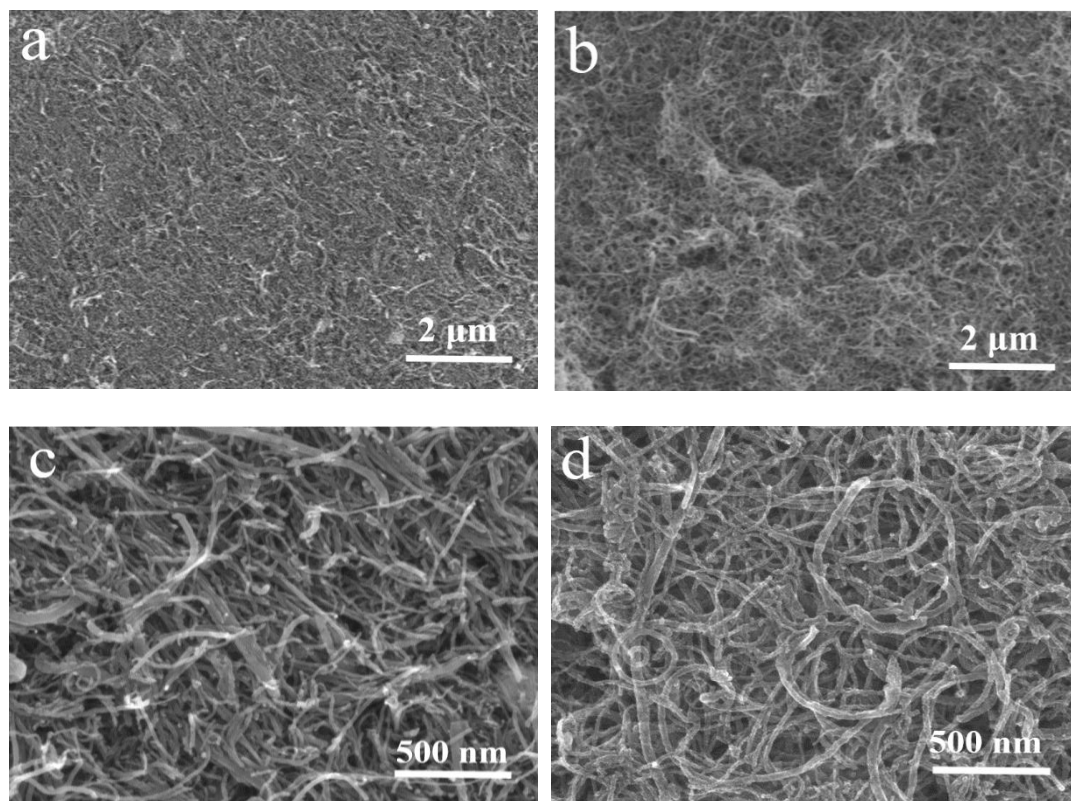


Figure S1. Typical SEM images of Sn/CNT (a, c) and Sn/CNT-Agls (b, d) (Figure S1d is the same as Figure 2b).

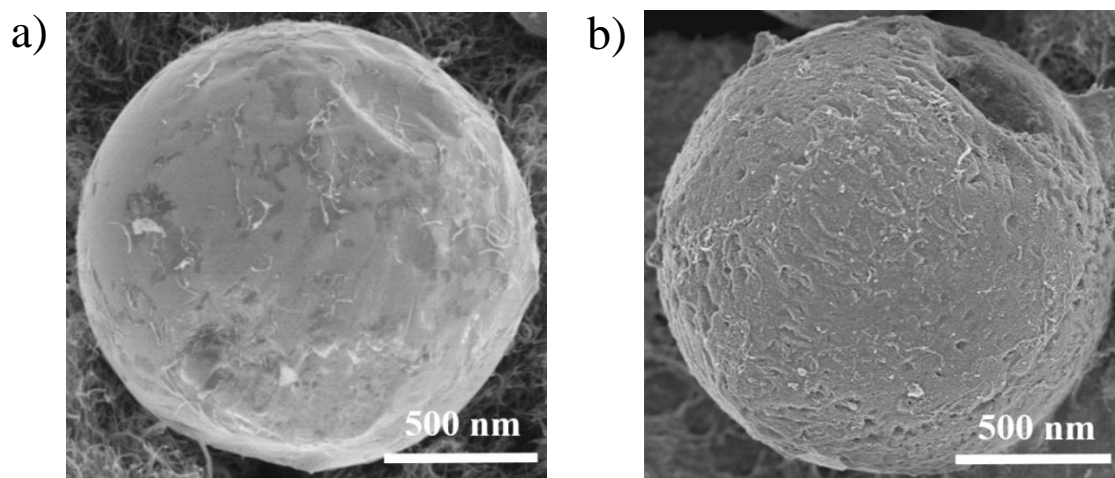


Figure S2. The morphology of the Sn particles supported on the CNT-Agls before (a) and after (b) the electrolysis experiment at -0.96 V.

The result indicate that the morphology of Sn particles did not change significantly during electrolysis. The surface roughness in Figure S2b is attributed to native thin SnO_x layer on the surface of Sn spheroidal particles being reduced to metallic Sn during electrolysis.

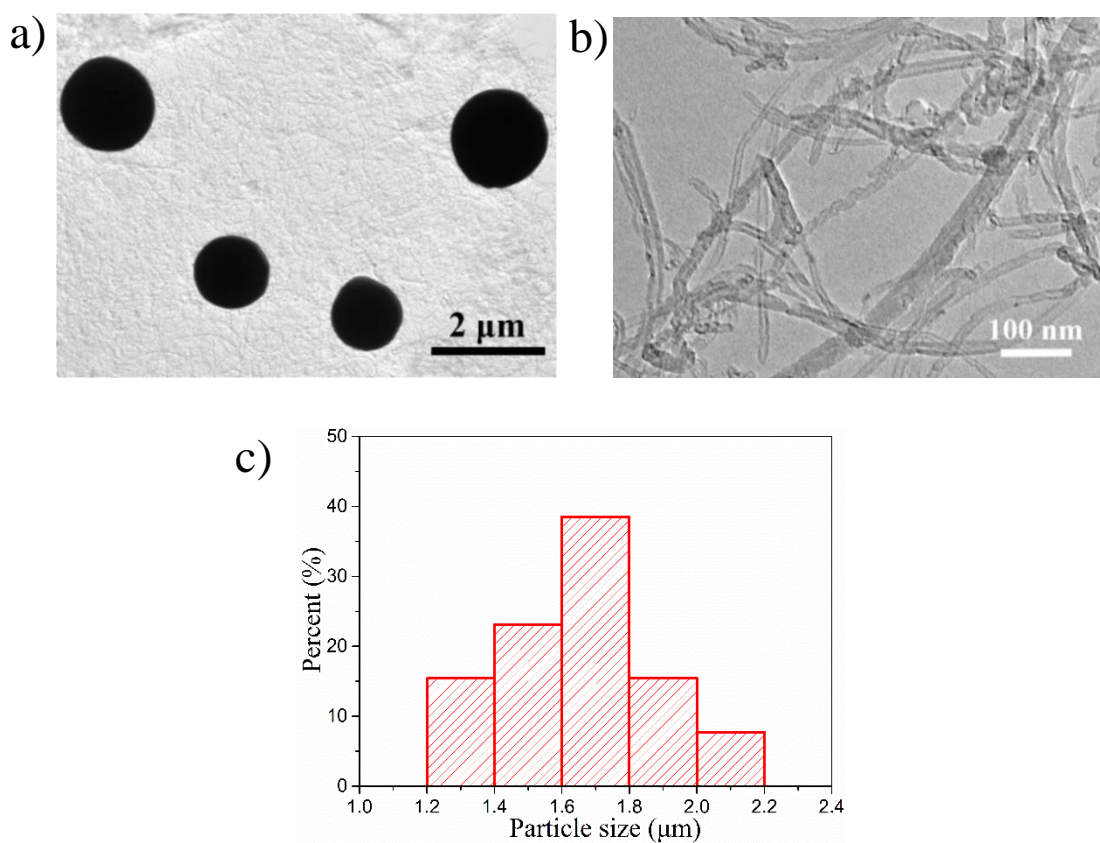


Figure S3. Typical TEM images of Sn/CNT-Agls (a, b) and the plot of Sn particles size distribution (c). No small Sn particles in the Sn/CNT-Agls were observed and the average size of Sn particles is 1.65 μm .

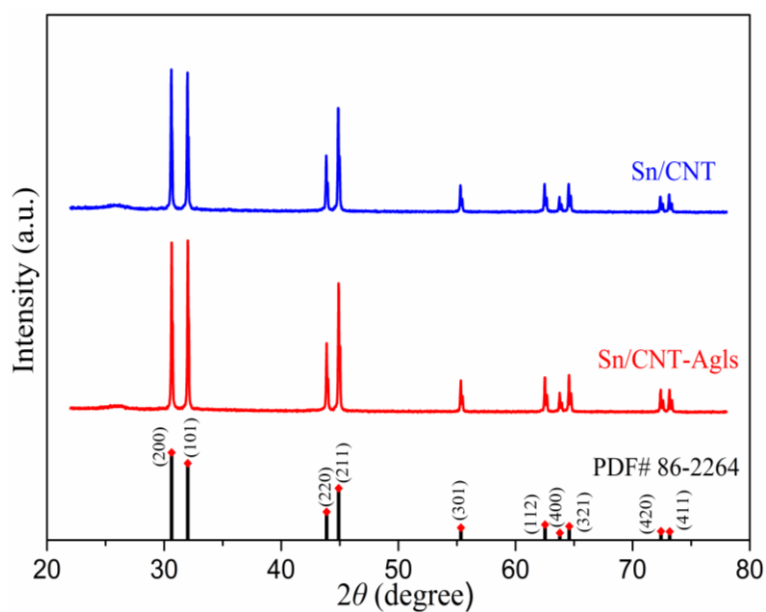


Figure S4. XRD patterns of the Sn/CNT and Sn/CNT-Agls samples

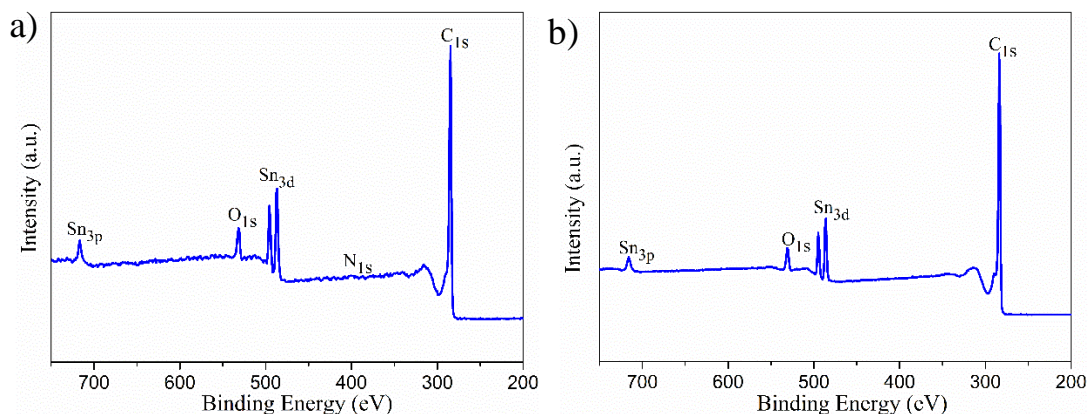


Figure S5. Survey XPS spectrum (a) Sn/CNT-Agls. (b) Sn/CNT.

The Survey XPS spectra of Sn/CNT-Agls and Sn/CNT are shown in Figure S5a and 5b, respectively. There are no significant differences between the Sn/CNT-Agls and Sn/CNT. The N is introduced by the addition of chitosan in in the synthesis of Sn/CNT-Agls.

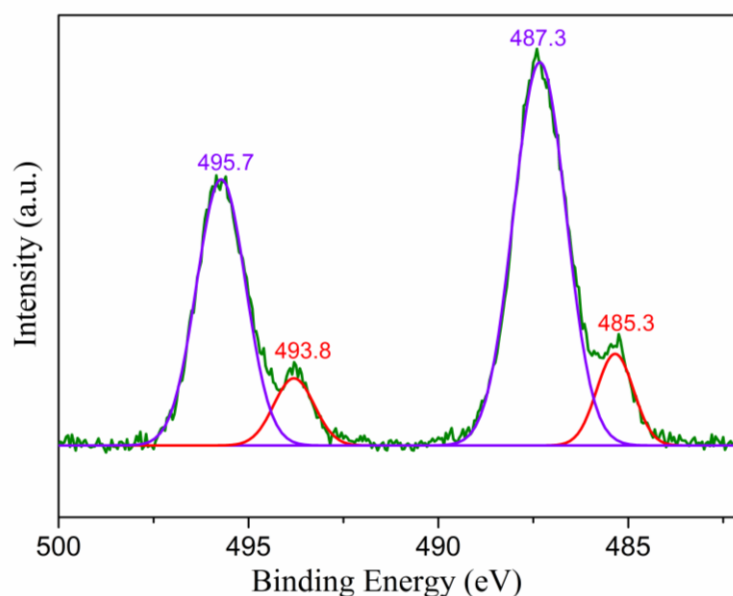


Figure S6. High-resolution Sn 3d XPS spectrum of Sn/CNT-Agls sample

The peaks at about 495.7 and 485.3 eV correspond to the $3d_{3/2}$ and $3d_{5/2}$ features of $\text{Sn}^{4+/2+}(\text{SnO}_x)$, respectively.^{1,2} This is attributed to the native SnO_x layer on the surface of the Sn particles which is formed in the air. A spin-orbital splitting energy of ca. 8.4 eV between the $3d_{3/2}$ and $3d_{5/2}$ orbitals was observed and it is consistent with previous

reported results.³ The integral results of the Sn 3d peaks exhibit a Sn⁰: SnO_x ratio of 18:82. The formal reduction potential of Sn⁴⁺/ Sn⁰ is -0.54 V (vs. NHE).⁴ Because the applied electrolysis potential of CO₂ reduction is far more negative than that formal reduction potential. Therefore, the native thin SnO_x layer on the surface of Sn spheroidal particles could be reduced to metallic state Sn⁰ during electrolysis. Consequently, the composition of Sn/CNT-Agls will not change significantly in the potential range of our experiment.

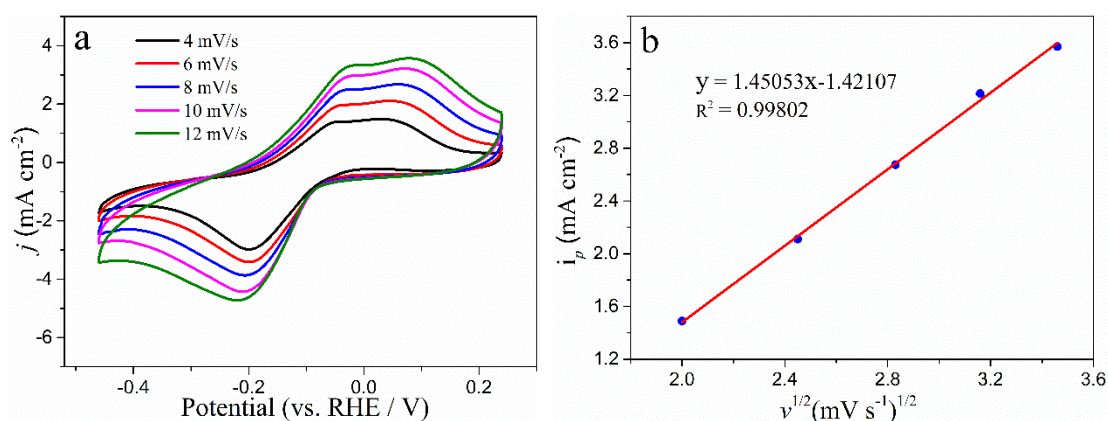


Figure S7. The cyclic voltammogram scanning results. (a) CVs of Sn/CNT-Agls/CC electrode measured at different sweep rate from 4 to 12 mV s⁻¹ in CO₂ saturated 0.5 M KHCO₃. (b) Variations of peak current densities with the sweep rates.

The control mechanism of electrochemical reaction at the Sn/CNT-Agls/CC electrode interface was investigated by the cyclic voltammograms at different sweep rates. It can be seen that the plot of peak current densities as a function of sweep rate is linear. The result confirms the electrochemical process is diffusion-controlled.^{5, 6} It should be attributed to the diffusion of reactants within the Sn/CNT-Agls/CC electrode rather than in the electrolyte.

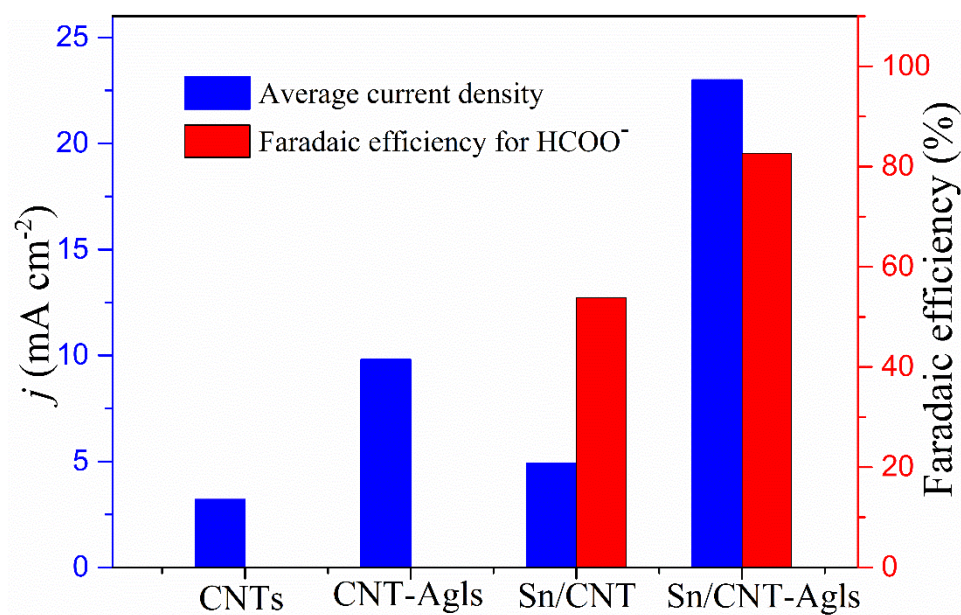


Figure S8. Comparison of average current density and Faraday efficiency of formate on CNTs/CC, CNT-Agls/CC, Sn/CNT/CC and Sn/CNT-Agls/CC electrodes at -0.96 V

Supplementary Table

Table S1. Comparison of electrocatalytic activity for electrochemical reduction of CO₂ to formate on Sn-based electrodes

Electrodes	Applied potential (V)	j_{total} (mA/cm ²)	Faradaic efficiency of formate (%)	Refs
Sn plate	-1.8 V vs. Ag/AgCl	2.5	91	7
OE-Sn plate	-1.8 V vs. Ag/AgCl	5.4	85	8
Sn rod	-1.76 V vs. Ag/AgCl	~8	60	9
Sn GDE	-1.8 V vs. Ag/AgCl	13.5	73	10
Electrodeposited Sn	-1.36 V vs. Ag/AgCl	15	91	11
Sn dendrite	-1.36 V vs. RHE	17.1	71.6	12
PTFE-Sn GDE	-1.8 V vs. Ag/AgCl	21.7	87	13
Sn GDE	-1.8 V vs. Ag/AgCl	22.2	78.6	14
Sn foam	-2.0 V vs. Ag/AgCl	23.5	90	15
Nafion-Sn GDE	-1.8 V vs. Ag/AgCl	27	70	16
Sn foil	-1.96 V vs. Ag/AgCl	28	63.5	17
Sn/CNT-Agls	-1.6 V vs. Ag/AgCl	26.7	82.7	This work
	(-0.96 V vs. RHE)			
	-1.8 V vs. Ag/AgCl	32.9	67.4	
	(-1.16 V vs. RHE)			

References

1. S. Zhang, P. Kang and T. J. Meyer, *J. Am. Chem. Soc.*, 2014, **136**, 1734-1737.
2. G. T. Baronetti, S. R. de Miguel, O. A. Scelza and A. A. Castro, *Applied catalysis*, 1986, **24**, 109-116.
3. W. K. Choi, H. J. Jung and S. K. Koh, *Journal of Vacuum Science & Technology A: Vacuum, Surfaces, and Films*, 1996, **14**, 359-366.
4. F. Li, L. Chen, G. P. Knowles, D. R. MacFarlane and J. Zhang, *Angew. Chem. Int. Ed.*, 2017, **129**, 520-524.
5. L. Siinor, J. Poom, C. Siimenson, K. Lust and E. Lust, *J. Electroanal. Chem.*, 2014, **719**, 133-137.
6. S. Sen, D. Liu and G. T. R. Palmore, *ACS Catal.*, 2014, **4**, 3091-3095.
7. W. Lv, R. Zhang, P. Gao and L. Lei, *J. Power Sources*, 2014, **253**, 276-281.
8. R. Zhang, W. Lv and L. Lei, *Appl. Surf. Sci.*, 2015, **356**, 24-29.
9. G. Frankel, A. Agarwal and N. Sridhar, *Electrochim. Acta*, 2014, **133**, 188-196.
10. Q. Wang, H. Dong and H. Yu, *RSC Advances*, 2014, **4**, 59970-59976.
11. C. Zhao and J. Wang, *Chem. Eng. J.*, 2016, **293**, 161-170.
12. D. H. Won, C. H. Choi, J. Chung, M. W. Chung, E. H. Kim and S. I. Woo, *ChemSusChem*, 2015, **8**, 3092-3098.
13. Q. Wang, H. Dong and H. Yu, *J. Power Sources*, 2015, **279**, 1-5.
14. Q. Wang, H. Dong and H. Yu, *J. Power Sources*, 2014, **271**, 278-284.
15. D. Du, R. Lan, J. Humphreys, S. Sengodan, K. Xie, H. Wang and S. Tao, *ChemistrySelect*, 2016, **1**, 1711-1715.
16. G. S. Prakash, F. A. Viva and G. A. Olah, *J. Power Sources*, 2013, **223**, 68-73.
17. J. Wu, F. Risalvato and X.-D. Zhou, *Ecs Transactions*, 2012, **41**, 49-60.